ELSEVIER

Materials Science and Engineering A335 (2002) 128–136

MATERIALS SCIENCE & ENGINEERING A

www.elsevier.com/locate/msea

Transformation-mismatch plasticity of NiAl/ZrO_2 composites—finite-element modeling

Peter Zwigl [a], David C. Dunand [b,*]

[a] *Intel Corp, Folsom, CA 95630, USA*

[b] *Department of Materials Science and Engineering, Northwestern University, 2225 North Campus Drive, Evanston, IL 60208-3108, USA*

Received 24 July 2001; received in revised form 29 October 2001

Abstract

A coupled thermo-mechanical finite-element model was developed to describe transformation-mismatch plasticity resulting from mismatch stresses produced by allotropic particles within a creeping matrix. A composite consisting of a NiAl matrix with 10 vol.% zirconia allotropic particles was modeled in two dimensions for a range of externally-applied stress values. The instantaneous composite strain developed during the zirconia transformation is found to increase linearly with the applied stress, in agreement with continuum-mechanical, closed-form models for transformation-mismatch plasticity. This instantaneous strain is smaller than the total strain accumulated over a half temperature cycle, indicating that mismatch stresses produced during the transformation relax by matrix creep long after the particles have transformed. Also, the total composite strain calculated after a full temperature cycle is in good agreement with strains determined experimentally on a NiAl–10% ZrO_2 composite. Finally, the internal stress distribution within the transforming composite is determined numerically and compared to simple analytical averages.

Keywords: Superplasticity; Phase transformations; Finite-element modeling; NiAl; ZrO_2

1. Introduction

When a uniaxial stress is applied on a polycrystalline material subjected to multiaxial internal stresses caused by an allotropic phase transformation, a strain increment develops in the direction of the externally-applied stress. This biasing phenomenon is called transformation-mismatch plasticity, or transformation-mismatch superplasticity when strains in excess of 100% are obtained through accumulation of individual strain increments each time a phase change occurs during thermal cycling. This deformation mechanism has been experimentally observed in pure metals and alloys [1,2], as well as metal–matrix composites based on these metals and alloys [3–6]. Recently, they were also observed in an intermetallic alloy (super-α2 titanium aluminide) cycled over its allotropic range [7]. In a previous experimental article [8], we reported that transformation-mismatch plasticity can be induced in the intermetallic composite NiAl–ZrO_2 through transformation of the ceramic particulate reinforcement within the creeping, non-transforming intermetallic matrix. Experimental results for different particle sizes, volume fractions and thermal cycling characteristics were found to obey the continuum mechanics model of Greenwood and Johnson [9] which can be expressed at small stresses as:

$$\Delta\varepsilon \approx \frac{2}{3}\left|\frac{\Delta V}{V}\right|\frac{\sigma}{\sigma_0}\frac{5n}{(4n+1)} \tag{1}$$

where $\Delta\varepsilon$ is the transformation-mismatch plasticity strain increment after a phase transformation, σ is the applied stress, $|\Delta V/V|$ is the average internal volume mismatch between the allotropic phases, σ_0 is the average internal stress of the creeping matrix, and n is the stress exponent of the creep law describing the plastic accommodation. Because Eq. (1) is only valid for single-phase, allotropic materials undergoing a complete phase transformation, an effective volume mismatch $(\Delta V/V)_{\text{eff}}$ was introduced in the case of the NiAl/ZrO_2 composite as [8]:

* Corresponding author. Tel.: +1-847-491-5370; fax: +1-847-467-6573.

E-mail address: dunand@northwestern.edu (D.C. Dunand).

0921-5093/02/$ - see front matter
PII: S0921-5093(01)01901-3

Table 1
Physical properties of ZrO_2 and NiAl used in the numerical model

Property	ZrO_2	Ref.	NiAl	Ref.
Density, ρ (g cm^{-3})	5.68 (monoclinic), 6.10 (tetragonal)	[17]	5.90	[18]
Enthalpy, ΔH (J g^{-1})	48.0	[19]	–	–
Specific heat, C_p (J g^{-1} K^{-1})	0.63	[20]	0.64 (527 °C), 0.68 (727 °C)[a]	[21]
CTE, $\alpha_{20\ °C}$ (K^{-1}) $\times 10^6$	6.92	[22]	14.5 (700 °C), 15.5 (1200 °C)	[23]
Thermal conductivity, k (W cm^{-1} K^{-1})	1.7 (100 °C), 2.1 (1300 °C)	[17]	78.6 (600 °C), 73.2 (1200 °C)	[24]
Poisson's ratio, ν	0.27	[19]	0.326 (600 °C), 0.329 (1300 °C)	[18]
Young's modulus, E (GPa)	303.8–0.108 T (K)	[19]	199.8–0.04 T (K)	[18]

[a] Assumed to remain at $C_p = 0.68$ J g^{-1} K^{-1} up to $T = 1200$ °C.

$$\left(\frac{\Delta V}{V}\right)_{\text{eff}} = f(1-f)\left|\frac{\Delta V}{V}\right| \quad (2)$$

Using this effective value in Eq. (1) takes into account that the only phase transforming in the composite is the ZrO_2 reinforcement with volume fraction f and allotropic mismatch $|\Delta V/V|$ between its monoclinic (m) and tetragonal (t) phases. Other approximations in Ref. [8] included using a lower transformation mismatch for the particle due to porosity, neglecting thermal expansion mismatch, and averaging strain increments and internal stresses over a full thermal cycle encompassing two transformations at different temperatures.

As compared to the continuum model with the above approximations, finite-element modeling allows a much more detailed description of the spatial distribution and temporal evolution of the internal stresses, and of the macroscopic strain increment history during the phase transformation. Ganghoffer et al. [10] modeled transformation plasticity of steel (austenite–pearlite) assuming a yielding, strain-hardening material showing no creep. Two-dimensional (2D) finite-element models were also used to investigate the problem of plasticity induced by the formation of martensite [11] or ferrite [12] within austenite. Finally, Zhang et al. [13,14] studied the related phenomenon of thermal mismatch plasticity in an Al–SiC composite subjected to thermal cycling, where internal stresses are produced by a mismatch in thermal expansion between the phases, rather than by an allotropic volume change. Their plane–strain, 2D model assumed an ideally plastic matrix with a mismatch which was approximated by radially shifting nodes at the reinforcement–matrix interface.

In the present paper, we use a coupled thermo-mechanical finite-element approach to model transformation-mismatch plasticity in the NiAl–ZrO_2 system, for which the intermetallic matrix is creeping and the ceramic reinforcement is undergoing a phase transformation. We compare our numerical, 2D, plane–strain results with experimental data presented in a previous paper [8].

2. Model

The physical properties of ZrO_2 and NiAl are presented in Table 1. The allotropic density change of zirconia, $|\Delta V/V|$, was modeled as a discrete non-linearity of the thermal expansion $|\Delta L/L| = |\Delta V/V|/3$ at the allotropic temperatures, as shown in Fig. 1. The particles are thus assumed to be polycrystalline with random texture, and to show only dilational strains upon transformation. The phase transformation of zirconia was assumed to take place within a temperature interval of ± 0.5 °C over which the transformation enthalpy is liberated or absorbed linearly. As observed experimentally for NiAl/ZrO_2 composites [8], transformation temperatures were taken as $T_{m/t} =$ 1076 °C on heating and at $T_{t/m} = 894$ °C on cooling; these values are lower than for unconstrained zirconia, because of matrix constraints [8].

The stress dependence of the creep strain rate $\dot{\varepsilon}$ of polycrystalline NiAl was described by a power-law:

$$\dot{\varepsilon} = A \exp\left(-\frac{Q}{RT}\right)\sigma^n \quad (3)$$

where the pre-exponential constant $A = 90$ MPa$^{-3.9}$, the activation energy $Q = 318$ kJ mol^{-1} and the stress exponent $n = 3.9$ were measured experimentally [8], and where R and T are the gas constant and temperature, respectively.

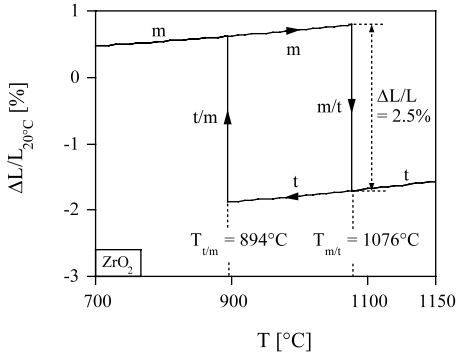

Fig. 1. Transformation hysteresis of zirconia used in model.

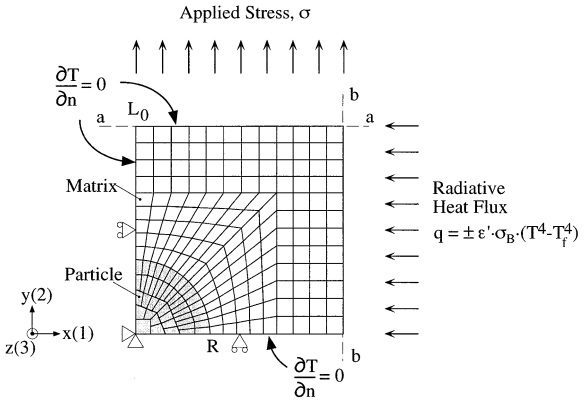

Fig. 2. Finite-element mesh showing boundary conditions and mechanical and thermal loads.

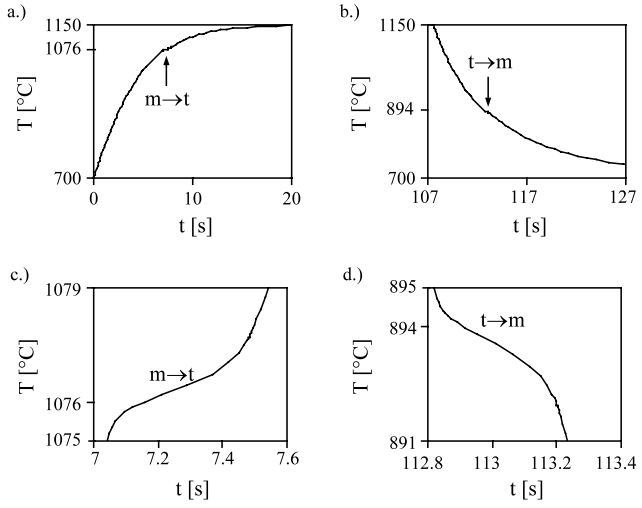

Fig. 3. Temperature profiles on heating (a) and cooling (b) with detailed views of the m/t (c) and t/m (d) transformation.

The finite-element code ABAQUS [15] was used with four-node, plane–strain, coupled temperature-displacement elements arranged in a domain shown in Fig. 2. The lower left corner of the mesh is fixed in space and the boundary conditions at the perimeter are set so that the domain remains rectangular. The round zirconia particle is modeled with 45 elements using multiple point constraints for the five elements near the origin, while the NiAl matrix is discretized with 160 elements. Continuity is maintained at the matrix/particle interface, which is thus assumed to be well-bonded at all times. A radiative heat flux controlled by the applied temperature profile in the form of a square wave (with a lower temperature T_l and an upper temperature T_u) is entering the domain along the b–b edge while a uniaxial stress is applied at the a–a boundary. The final stress state at the end of each transformation (heating or cooling) was used as the initial state for the succeeding calculations, using a user-defined routine to transfer the stresses. To minimize the distortions of the elements caused by repeated transformations, the original, undistorted mesh was used as input geometry for each segment. The composite strain was calculated as the ratio of the upper a–a boundary displacement in the y-direction to the length of the domain (arbitrarily set to $L_0 = 252$ μm).

A thermal cycle consisted of a heating segment followed by a cooling segment. The heating segment resulting from the applied square wave heat-flux was implemented in three steps: (i) heating from the lower cycle temperature $T_l = 700$ °C to the phase transformation temperature T_p; (ii) transformation at T_p over a temperature interval of $\Delta T = 1$ K; and (iii) heating from T_p to the upper cycling temperature $T_u = 1150$ °C. Smaller temperature-, strain-, and time increments were used during the transformation (step (ii)). The same three steps were repeated during the cooling segment of the temperature cycle. A total of three complete thermal cycles, each spanning 214 s, were calculated to allow for dynamic equilibrium of stresses. The initial stress state at the beginning of the first cycle was different from that of the second cycle. However, there was very little difference between the second and the third cycle. Thus, the simulation was not carried out past the third cycle, which was used to determine the strain increment.

3. Results

Fig. 3a–d show the temperature history during a temperature cycle, as measured at the upper left corner of the domain (Fig. 2). Upon heating (Fig. 3a), the temperature increases rapidly until the onset of the phase transformation of the zirconia particle. During the transformation which lasts about 0.5 s. (Fig. 3c), some of the incoming heat is used for the transformation enthalpy of the particle, thus reducing the average rate of heating. After completion of the transformation, the final temperature increases again rapidly. Conversely, on cooling (Fig. 3b), the heat released by the phase transformation reduces the rate of cooling until completion of the transformation (Fig. 3d).

Fig. 4 shows the strain histories of the composite for four different applied stress levels, as determined from the deformation of the upper edge of the domain. The initial elastic response of the composite is $E = 187$ GPa at $T = 700$ °C, comparing well with $E = 161$ GPa for NiAl and $E = 199$ GPa for pure zirconia at that temperature (Table 1). The non-linearities at $t = 7$ s and $t = 113$ s are caused, respectively, by the m/t and t/m phase transformations. The thermal and allotropic expansion and contraction cancel over a full cycle, as shown by the zero strain value at the end of the cycle for $\sigma = 0$ MPa in Fig. 4. On the other hand, the strains caused by the biasing of the internal mismatch stresses

through the externally applied stress accumulate into an irreversible plastic strain increment over a cycle, visible as a strain offset at the end of the cycle for curves with $\sigma > 0$ MPa in Fig. 4.

This effect is illustrated more clearly in Fig. 5a, where the strain history of Fig. 4 for $\sigma = 0$ MPa (which consists only of reversible thermal and allotropic strains) has been subtracted from the strain histories for $\sigma = 10$, 20 and 30 MPa. The resulting differential curves in Fig. 5a thus show only the irreversible plastic deformation during cycling. During the heating part of the cycle, a strain spike is observed upon the m/t transformation, followed by creep strain accumulation at T_u, which increases with increasing stress. Upon subsequent cooling, the strain spike due to the t/m transformation is followed by a region of zero creep as the temperature T_e is too low for NiAl to deform appreciably. The total strain increment after a full cycle thus consists of contribution from both transformation-mismatch plasticity and isothermal creep at T_u.

Fig. 5b shows details of the strain curves of Fig. 5a in the vicinity of the phase transformation, which are superimposed for both heating and cooling transformations for comparison purpose, with $t = 0$ the start of the heating or cooling segment. On cooling, a short interval of creep accumulation (~ 6 s) precedes the strain spike due to the t/m transformation. This strain spike is followed by a 5-s interval where creep is faster than before the transformation, despite the lower temperature. During this interval, allotropic mismatch stresses are relaxing under the biasing effect of the applied stress to produce the increased creep rate. Finally, the creep rate becomes insignificant, as expected from steady-state creep at this low temperature. On heating, after approximately 7 s of creep, the m/t transformation strain spike takes place, which is larger than the t/m strain spike on cooling. The spike is also followed by an 8-s interval where creep is faster than the steady-state value at the maximum temperature, again due to the biased relaxation of transformation mismatch stresses. Finally, we note that for both heating and cooling, the strain rate before the transformation spike is higher than expected based only on steady-state creep (as can also be seen in Fig. 5a). This phenomenon can be explained by internal stresses produced by the thermal expansion mismatch between matrix and particles, as modeled by Zhang et al. [13,14] for thermally-cycled Al–SiC composites. The plastic strains associated with this phenomenon are however small as compared to those induced by the allotropic transformation of the particle.

The instantaneous composite strain occurring during zirconia transformation is given by the difference between the maxima and minima of the strain spikes

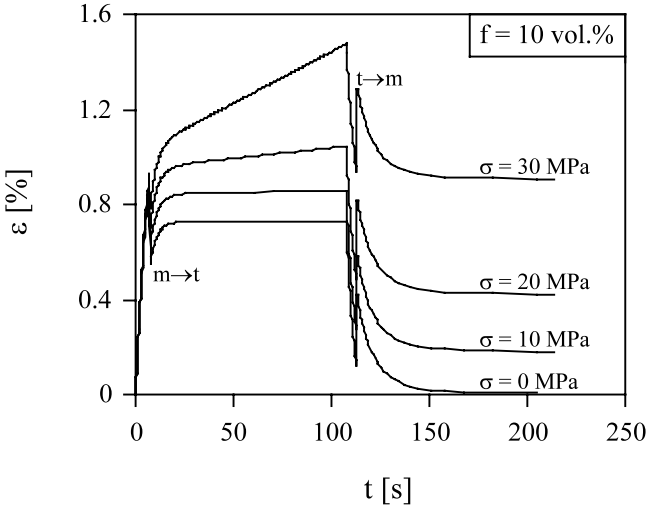

Fig. 4. Strain histories of NiAl/10%ZrO_2 composite at different applied stresses.

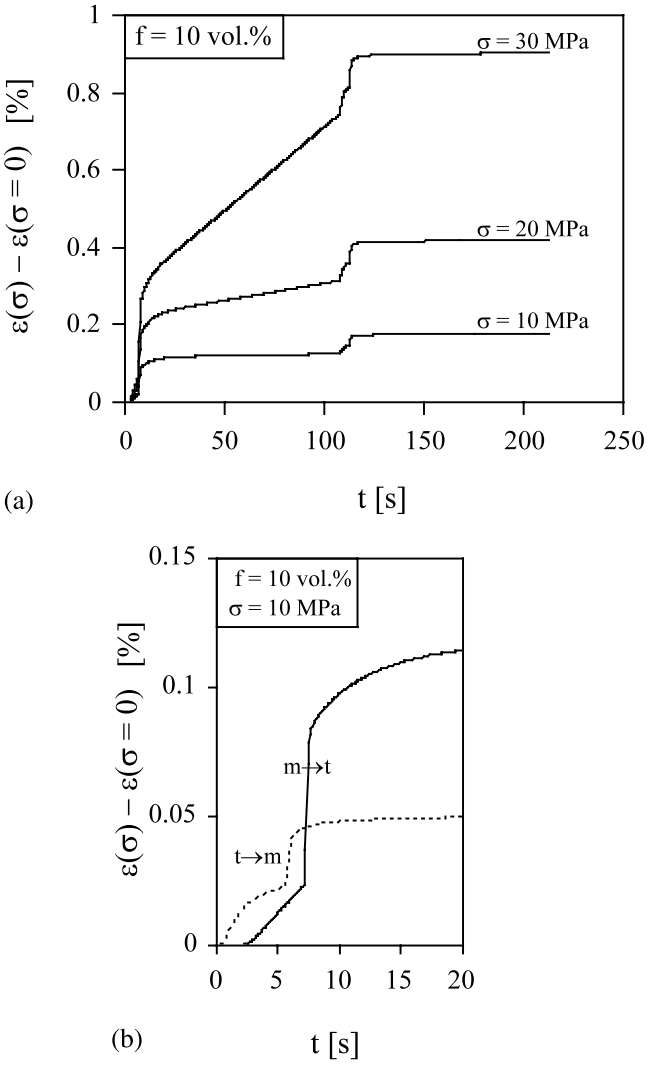

Fig. 5. (a) Plastic strain history from Fig. 4 (with strain history for 0 MPa subtracted) and (b) plastic strain history for the first 20 s. of heating and cooling, showing the phase transformations.

visible in Fig. 4. These instantaneous strains (as well as their sum) are plotted as a function of the applied stress in Fig. 6 for the t/m and m/t transformations. Fig. 6 shows linear relations for the m/t-transformation (with slope $d(\Delta\varepsilon_{m/t})/d\sigma = 0.053\ GPa^{-1}$) and the t/m transformation (with slope $d(\Delta\varepsilon_{t/m})/d\sigma = 0.015\ GPa^{-1}$), which have similar intercept magnitude of $\Delta\varepsilon_{0,m/t} = -0.305\%$ and $\Delta\varepsilon_{0,t/m} = 0.299\%$, corresponding to the values obtained for zero applied stress.

Fig. 7 shows contour plots of Mises equivalent matrix stress before, during, and after the m/t phase transformation on heating. The maximum matrix equivalent stress found at the particle–matrix interface just before the transformation is $\sigma = 67$ MPa (Fig. 7b); this relatively high value is attributed to thermal expansion mismatch during heating, which produces the enhanced strain rate described above. As the zirconia particle shrinks during the m/t transformation, the maximum stress rises (Fig. 7c,d) to finally reach a value of $\sigma = 240$ MPa at the end of the transformation (Fig. 7e). Upon subsequent creep (Fig. 7f), the matrix stresses relax and drop to values on the order of the applied stress ($\sigma = 10$ MPa). Similar stress distributions were obtained during cooling, but with higher maximum stresses (up to 800 MPa) because the matrix is stronger at the lower transformation temperature.

Finally, Fig. 8 shows the isothermal creep strain rate as a function of applied stress for unreinforced NiAl and the NiAl–10vol.%ZrO_2 composite at $T = 1150$ °C. For NiAl, plane–strain creep was simulated by using 4×4 plane–strain square elements with the same boundary conditions as in Fig. 2. Isothermal creep rates obtained analytically (Eq. (3)) and numerically are in excellent agreement. The composite creep rate was determined from the deformation rate at upper cycling

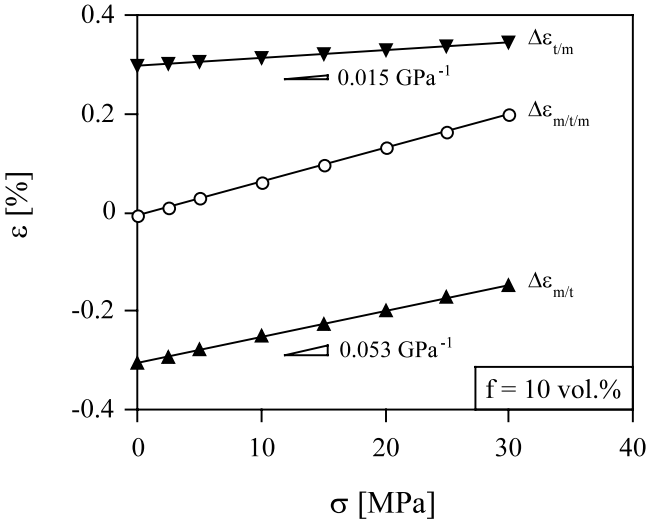

Fig. 6. Instantaneous strain increment after transformation as a function of applied stress for the individual m/t and t/m transformation and the sum of both transformations

temperature $T_u = 1150$ °C just before cooling occurred. As qualitatively expected, the composite creeps more slowly than the unreinforced matrix; the creep rate difference is, however, very small, indicating that load transfer from the creeping matrix to the elastic particles is inefficient.

4. Discussion

4.1. Thermal behavior

The principal characteristics of the heating and cooling curves (Fig. 3a–d) are compared to simple analytical predictions in the following. Similar to the Biot number for conductive heat transport, a dimensionless number can be defined for radiative heat transfer [16]:

$$M = \frac{\sigma_B \alpha T^3 x}{k} \tag{4}$$

where σ_B is the Stefan–Boltzmann constant, k is the thermal conductivity, α is the absorbtivity (replaced by emissivity ε on cooling) and x is the thermal diffusion distance (taken as the domain size for NiAl and the particle radius for ZrO_2). Assuming $\alpha = \varepsilon = 0.5$ and taking thermal properties of the matrix (Table 1), Eq. (4) gives M values smaller than 0.01, i.e. no thermal gradients are expected, so that ratchetting from macroscopic thermal gradients can be excluded as a deformation mechanism. The calculated temperature difference between the center of the particle and the upper left corner of the matrix domain is negligible outside the transformation range and at most 1 K during the phase transformation, consistent with the low values of M predicted by Eq. (4).

Under isothermal conditions, energy balance can be written as:

$$\rho C_p V \frac{dT}{dt} = -S\sigma_B \alpha (T^4 - T_f^4) \tag{5}$$

where ρ is the density, C_p the specific heat, V the volume to be heated, S the surface area for heat transfer and T_f the applied surface temperature. Solving Eq. (5) for the initial condition $T(t=0) = T_i$ gives an analytical expression for the temperature history, from which the time interval Δt_r to heat a material from an initial temperature T_i to a temperature T can be found as:

$$\Delta t_r = \frac{\rho C_p V}{4 S \sigma_B \alpha T_f^3}\left\{2\arctan\left[\frac{T_f(T - T_i)}{T_f^2 + T T_i}\right] + \ln\left[\frac{(T + T_f)(T_i - T_f)}{(T - T_f)(T_i + T_f)}\right]\right\} \tag{6}$$

Given an applied temperature $T_f = 1150$ °C, the time interval to heat the domain from the initial temperature of 700 °C to the beginning of the phase transformation

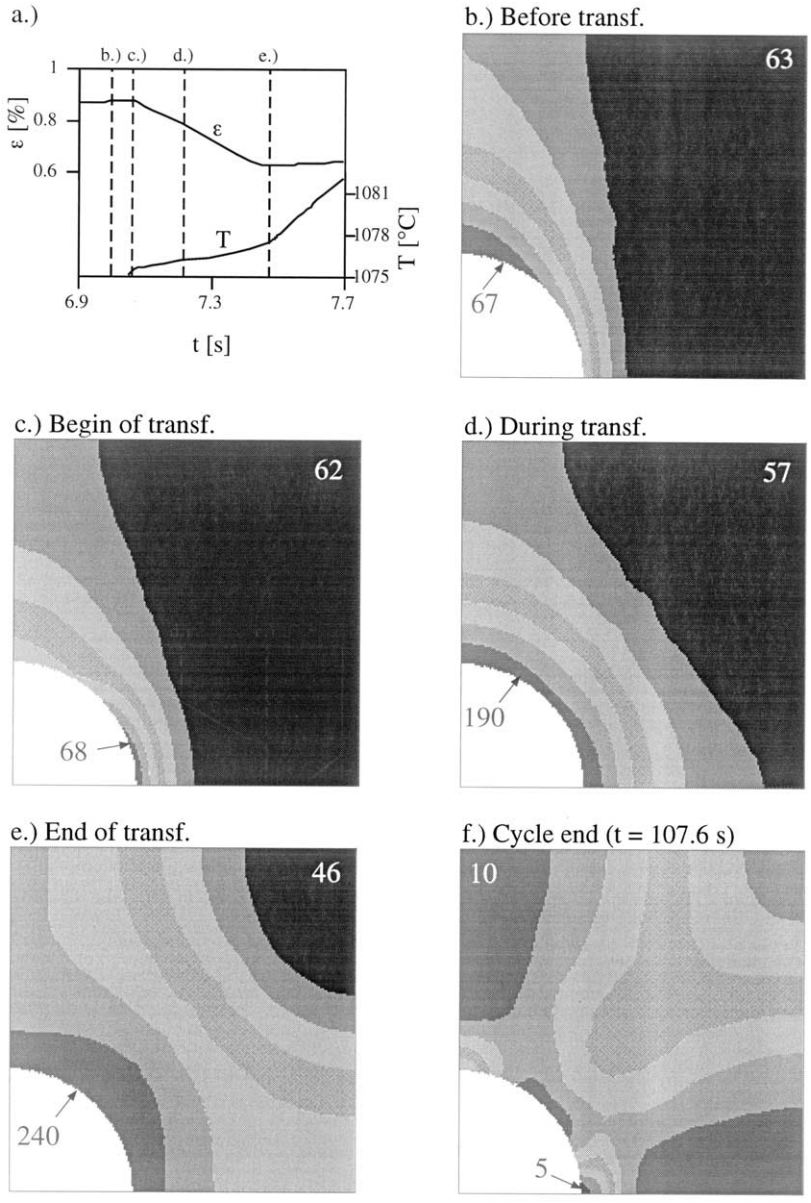

Fig. 7. Mises equivalent matrix stress contours at different times before, during and after the transformation with a superimposed external stress of 10 MPa in the vertical direction. Gray levels indicate approximately equidistant stress regions; maximum and minimum values are marked in MPa units.

(1075.5 °C) is given by Eq. (6) as $\Delta t_{r1} = 7.0$ s, which compares well with the value found numerically $\Delta t_{r1} = 7.1$ s. Upon cooling from 1150 °C to the t/m phase transformation temperature (894.5 °C), Eq. (6) predicts $\Delta t_{r2} = 5.2$ s, again in good agreement with the numerical result $\Delta t_{r2} = 5.3$ s.

Under Newtonian conditions, the time interval Δt_p needed to complete the phase transformation is:

$$\Delta t_p = \frac{fV\rho\Delta H}{S\sigma_B\alpha(T_f^4 - T_p^4)} \quad (7)$$

which is found by replacing in Eq. (5) the term $C_p\Delta t$ with $f\Delta H$ (where f is the volume fraction of allotropic material and ΔH its enthalpy of transformation) and setting $T = T_p$ (where T_p is the phase transformation temperature). The transformation times defined by the strain spikes in Fig. 4 are found as $\Delta t_{p,m/t} = 0.42$ s and $\Delta t_{p,t/m} = 0.39$ s, close to the values of $\Delta t_{p,m/t} = 0.32$ s and $\Delta t_{p,t/m} = 0.26$ s predicted by Eq. (7) using $fV/S = \pi R^2/(4L_0)$, i.e. assuming that heat enters along the b–b edge of the matrix domain (Fig. 2). The numerical values are expected to be higher than predicted analytically, as heat flow through the matrix is neglected.

4.2. Thermomechanical behavior

Fig. 6 displays the strain accumulated during the time of the transformation upon heating and upon

cooling defined by the spikes in Fig. 4 (points (c) and (e) in Fig. 7 for heating). As expected, the intercepts for zero applied stresses $|\Delta\varepsilon_{0,m/t}| = 0.305\%$ and $\Delta\varepsilon_{0,t/m} = 0.299\%$ are the same within numerical error, i.e. the composite expands and contracts reversibly when no external stress is applied. The magnitude of this strain, $\Delta\varepsilon_0 = 0.30\%$, can be compared to the composite effective volume mismatch given by Eq. (2) with $f = 0.1$ as $(\Delta V/V)_{eff} = 0.675\%$. The corresponding uniaxial expansion or contraction are $(\Delta V/V)_{eff}/3 = 0.225\%$ for an unconstrained material, and $(\Delta V/V)_{eff}/2 = 0.338\%$ for a material fully constrained in one direction, as in our plane–strain calculations. The slightly lower value of $\Delta\varepsilon_0 = 0.30\%$ determined numerically indicates that some small elastic strains are stored in the material. In addition, internal stresses are caused by the CTE-mismatch between the particle and the matrix. However, the effect of these internal stresses is negligible because the allotropic mismatch is much larger than the equivalent volumetric CTE-mismatch, as shown in our earlier article [8]. Finally, we note that the experimentally-determined transformation strains ($|\Delta L/L| = 0.10$–0.13% [8]) are significantly smaller, most probably because porosity allows for some free expansion and contraction of the particles during the transformation.

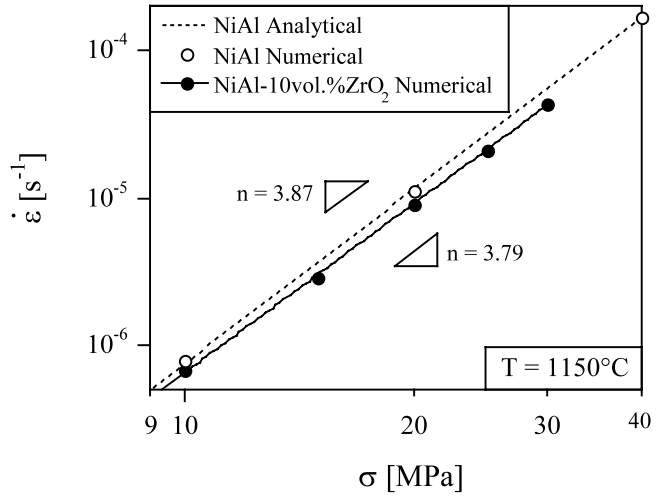

Fig. 8. Isothermal steady-state creep rate as a function of the applied stress at the upper cycling temperature of NiAl and a NiAl–10%ZrO_2 composite.

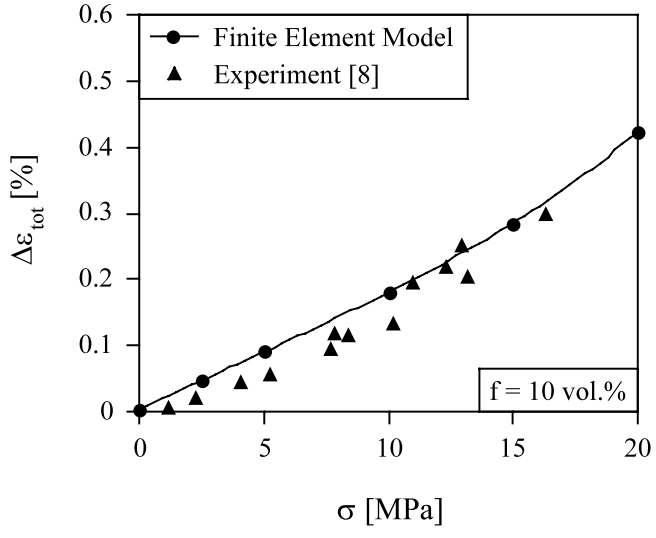

Fig. 9. Strain increment per cycle calculated numerically and measured experimentally [8] for a NiAl–10%ZrO_2 composite.

In Fig. 6, the slope of the strain increment vs. stress lines on heating $d(\Delta\varepsilon_{m/t})/d\sigma = 0.053\ GPa^{-1}$ is much larger than on cooling $d(\Delta\varepsilon_{t/m})/d\sigma = 0.015\ GPa^{-1}$. This is expected, as the transformation temperature is higher on heating ($T_{m/t} = 1076$ °C) than on cooling ($T_{t/m} = 894$ °C), and thus more elastic strains are stored on cooling, leading to lower plastic strains. Finally, the slope of the total strain per cycle in Fig. 6 $d(\Delta\varepsilon_{m/t/m})/d\sigma = 0.068\ GPa^{-1}$ can be compared to the experimental value $d(\Delta\varepsilon)/d\sigma = 0.13$–$0.15\ GPa^{-1}$, the transformation-mismatch strain (without creep contribution) accumulated over a complete cycle as measured for a NiAl–10%ZrO_2 composite [8]. Assuming that the 2D plane–strain model accurately describes the transformation in the composite, the discrepancy of a factor of two can again be justified with the argument that the strain does not develop fully during the short time when zirconia transforms ($\Delta t_p = 0.4$ s), but that stored transformation elastic strains relax under the biasing effect of the external stress during the rest of the cycle.

To test this hypothesis, the calculated total strain $\Delta\varepsilon_{tot}$ accumulated over a full cycle (Fig. 4) is compared in Fig. 9 with experimental data for NiAl–10%ZrO_2 composites cycled between $T_l = 750$ °C and $T_u = 1150$ °C [8] with applied heating/cooling ramps lasting 1 min and hold times of 1 min at T_l and T_u. Despite minor differences in the heating/cooling profiles, the 2D model predictions and the experimental data show surprisingly good match with each other. The model predicts quite well both the initial slope $d(\Delta\varepsilon_{tot})/d\sigma$ and the non-linear deviation occurring at high applied stresses, which corresponds to the onset of a significant contribution of creep during the high-temperature section of the cycle.

Finally, Fig. 10a,b show the effect upon the strain increment of the two variables affecting the effective mismatch (Eq. (2)): the volume fraction f (varied between 2.5 and 25 vol.% in Fig. 10a) and the transformation mismatch $\Delta V/V$ (varied between 2.5 and 7.5% in Fig. 10b). In Fig. 10a,b, both the instantaneous strain increment accumulated during the transformations $\Delta\varepsilon_{m/t/m}$ and the total strain increment accumulated over the whole cycle $\Delta\varepsilon_{tot}$ are plotted. In good agreement with Eqs. (1) and (2), the strain increments are linearly proportional to both variables f and $|\Delta V/V|$ (the probable cause for deviations observed for $f > 20$ vol.% is the

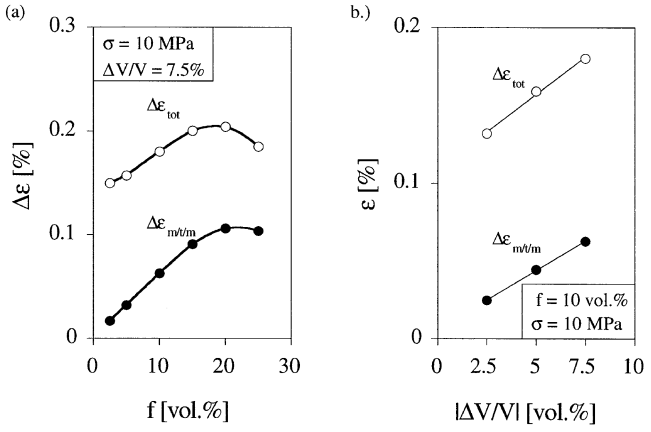

Fig. 10. Total strain increment per cycle and instantaneous strain increment as a function of (a) ZrO_2 volume fraction f at constant $\Delta V/V = 7.5\%$ and (b) ZrO_2 volume mismatch $\Delta V/V$ at constant volume fraction $f = 10$ vol.%.

significant overlap in stress field between neighboring particles). Also as expected from Eqs. (1) and (2), the instantaneous strain increment $\Delta\varepsilon_{m/t/m}$ extrapolates to zero when either variable f or $\Delta V/V$ tends to zero. The shift of about 0.1% between $\Delta\varepsilon_{tot}$ and $\Delta\varepsilon_{m/t/m}$ corresponds in large part to isothermal creep accumulated during the cycle outside the transformation range.

4.3. Internal stresses

Within the linear range in Fig. 9 ($\sigma \leq 10$ MPa) where the contribution of creep outside the transformation range is small enough to be neglected, slopes of $d(\Delta\varepsilon)/d\sigma$ for heating and cooling segments can be evaluated separately, giving $d(\Delta\varepsilon_h)/d\sigma = 0.125\ GPa^{-1}$ and $d(\Delta\varepsilon_c)/d\sigma = 0.051\ GPa^{-1}$, respectively. Because $\Delta\varepsilon_h$ and $\Delta\varepsilon_c$ incorporate stress relaxation over a much longer period, the resulting slopes are higher than those obtained from strain spikes ($d(\Delta\varepsilon_{m/t})/d\sigma = 0.053\ GPa^{-1}$ and $d(\Delta\varepsilon_{t/m})/d\sigma = 0.015\ GPa^{-1}$, Fig. 6). With the heating and cooling segment slopes and the effective mismatch defined by Eq. (2), Eq. (1) can be used to determine the average internal stress σ_0 in the NiAl matrix due to transformation mismatch strains, giving values $\sigma_{0,h} = 42$ MPa and $\sigma_{0,c} = 104$ MPa for heating and cooling, respectively.

Alternatively, the average internal stress can be calculated using the method of Greenwood and Johnson [9]:

$$\sigma_0 = \left(\frac{2}{3}\left|\frac{\Delta V}{V}\right|_{eff}\frac{\exp(Q/RT)}{A\Delta t^*}\right)^{1/n} \quad (8)$$

where Δt^* is the transformation time for a pure allotropic material. For the NiAl–10%ZrO_2 composites, Δt^* corresponds to the time during which internal stresses are large. Using a lower bound $\Delta t^* = \Delta t_p$, Eq. (8) yields upper bounds for the internal stresses $\sigma_{0,m/t} = 142$ MPa and $\sigma_{0,t/m} = 449$ MPa. The rather broad ranges of internal stresses given by Eqs. (1) and (8) (42–142 MPa on heating and 104–449 MPa on cooling) correspond to averages over the whole matrix volume stress and over the complete relaxation time. While they are thus not directly comparable to the instantaneous internal stresses determined numerically, these average values obtained from Eqs. (1) and (8) are of similar magnitude as those found by finite-element modeling in Fig. 7c–e.

5. Conclusions

Transformation-mismatch plasticity (resulting from the biasing by an external stress of internal mismatch stresses produced by an allotropic transformation) was modeled numerically for a NiAl–10%ZrO_2 composite, where the ceramic reinforcement is allotropic and the intermetallic matrix deforms by creep. The two-dimensional, plane–strain, finite-element model provides the following insights.

(a) The coupled thermo-mechanical formulation captures the temperature history expected for a transforming composite without thermal gradients.

(b) The composite strain developed over the short time interval (~ 0.4 s) where the zirconia particles undergo their phase transformation and produce high internal stresses is found to increase linearly with the applied stress, in qualitative agreement with the analytical expression developed by Greenwood and Johnson [9] for transformation-mismatch plasticity. Composite strain is found to accumulate even after the end of the transformation, as the decay of mismatch stresses is slower than the transformation.

(c) The total composite strain accumulated over a full temperature cycle increases linearly with stress for low stress values, as expected for transformation-mismatch plasticity, but becomes non-linear at high stresses because of the contribution of isothermal creep. The numerical predictions are in good agreement with experimental data in both the linear and non-linear regions, despite the simplifications used in the model.

(d) The internal matrix stress distribution was computed before, during, and after the phase transformation. Large internal stresses are produced during the phase transformation, in general agreement with average values determined analytically. Significant internal mismatch stresses still exist at the end of the phase transformation, as expected from the observation that strain accumulates even after the transformation ends.

Acknowledgements

This study was supported by the US Army Research Office (grant DAAH004-95-1-0629) when both authors

were in the Department of Materials Science and Engineering of the Massachusetts Institute of Technology. DCD further acknowledges the support of AMAX in the form of a career development chair at MIT. The authors also thank Professor H. Lehar (Innsbruck University) and Dr. C. Schuh (Northwestern University) for useful discussions as well as the computer center of Innsbruck University on which computers all calculations were performed.

References

[1] T.G. Nieh, J. Wadsworth, O.D. Sherby, Superplasticity in Metals and Ceramics, Cambridge University Press, Cambridge, UK, 1997.
[2] D.C. Dunand, in: T. Chandra, T. Sakai (Eds.), International Conference on Thermomechanical Processing of Steels and Other Materials, TMS, Warrendale, PA, 1997, pp. 1821–1830.
[3] D.C. Dunand, C.M. Bedell, Acta Mater. 44 (1996) 1063–1076.
[4] C. Schuh, D.C. Dunand, Scripta Mater. 40 (1999) 1305–1312.
[5] C. Schuh, D.C. Dunand, Int. J. Plastic. 17 (2001) 317–340.
[6] P. Zwigl, D.C. Dunand, Metall. Mater. Trans. 29 (1998) 565–575.
[7] C. Schuh, D.C. Dunand, Acta Mater. 46 (1998) 5663–5675.
[8] P. Zwigl, D.C. Dunand, Mater. Sci. Eng. 298 (2001) 63–72.
[9] G.W. Greenwood, R.H. Johnson, Proc. R. Soc. Lond. A 283 (1965) 403–422.
[10] J.F. Ganghoffer, S. Denis, E. Gautier, A. Simon, S. Sjostrom, Eur. J. Mech. A/Solids 12 (1993) 21–32.
[11] V.I. Levitas, E. Stein, A.V. Idesman, J. Phys. IV 6 (1996) C1-309–C1-314.
[12] P. Zwigl, D.C. Dunand, Mater. Sci. Eng. A262 (1999) 166–172.
[13] H. Zhang, G.S. Daehn, R.H. Wagoner, Scripta Metall. Mater. 24 (1990) 2151–2155.
[14] H. Zhang, G.S. Daehn, R.H. Wagoner, Scripta Metall. Mater. 25 (1991) 2285–2290.
[15] Hibbet, Karlsson, Sorensen, ABAQUS (version 5.5), Providence RI, vol. pp.
[16] D.R. Geiger, G.H. Poirier, Transport Phenomena in Materials Processing, TMS, Warrandale, PA, 1994.
[17] M.B. Bever (Ed.), Encyclopedia of Materials Science and Engineering, Pergamon Press, Oxford, 1986.
[18] R.D. Noebe, R.R. Bowman, M.V. Nathal, Intern. Mater. Rev. 38 (1993) 193–232.
[19] J. Shackelford, W. Alexander (Eds.), The CRC Materials Science and Engineering Handbook, CRC Press, Boca Raton, FL, 1992.
[20] Y.S. Touloukian (Ed.), Thermal Conductivity of Metallic Elements and Alloys, IFI/Plenum, New York, 1970.
[21] D.B. Miracle, Acta Metall. Mater. 41 (1993) 649–684.
[22] Y.S. Touloukian, R.K. Kirby, R.E. Taylor, P.D. Desai (Eds.), Thermal Expansion: Nonmetallic Solids, Plenum, New York, 1977.
[23] R.W. Clark, J.D. Whittenberger, in: T.A. Hahn (Ed.), Thermal Expansion 8, Gaithersburg, Plenum Press, New York, 1981, pp. 189–196.
[24] R. Darolia, J. Metals 43 (1991) 44–49.